Structure and Decompression Melting of a Novel, High-Pressure Nanoconfined 2-D Ice

Jianwei Wang,* Andrey G. Kalinichev, and R. James Kirkpatrick

Department of Geology, University of Illinois at Urbana-Champaign, Urbana, Illinois 61801

Received: October 14, 2004; In Final Form: May 5, 2005

Molecular dynamics (MD) simulations of water confined in nanospaces between layers of talc (system composition $Mg_3Si_4O_{10}(OH)_2 + 2H_2O$) at 300 K and pressures of approximately 0.45 GPa show the presence of a novel 2-D ice structure, and the simulation results at lower pressures provide insight into the mechanisms of its decompression melting. Talc is hydrophobic at ambient pressure and temperature, but weak hydrogen bonding between the talc surface and the water molecules plays an important role in stabilizing the hydrated structure at high pressure. The simulation results suggest that experimentally accessible elevated pressures may cause formation of a wide range of previously unknown water structures in nanoconfinement. In the talc 2-D ice, each water molecule is coordinated by six O_b atoms of one basal siloxane sheet and three water molecules. The water molecules are arranged in a buckled hexagonal array in the $a-b$ crystallographic plane with two sublayers along [001]. Each H_2O molecule has four H-bonds, accepting one from the talc OH group and one from another water molecule and donating one to an O_b and one to another water molecule. In plan view, the molecules are arranged in six-member rings reflecting the substrate talc structure. Decompression melting occurs by migration of water molecules to interstitial sites in the centers of six-member rings and eventual formation of separate empty and water-filled regions.

Introduction

Water confined in nanospaces exhibits complex and incompletely understood phase behavior and physical properties that can be quite different than those of bulk liquid water and crystalline ice.[1−11] The effects of water confinement play important roles in many chemical, geological, and biological processes, such as hydration and reactivity of mineral surfaces in natural environments, hydrophobic interactions of peptides and lipid membranes, and the stability of tissues below the point of ice crystallization due to freezing point depression in the vicinity of macromolecules and membranes.[12−15] In recent years, these effects have been extensively studied experimentally[13,16,17] and computationally.[18−26] The confinement-induced changes in the water structure and dynamics are commonly substrate-specific because the substrate−water interaction spatially restricts the translational and rotational mobility of individual H_2O molecules and may also cause significant water−substrate hydrogen bonding. For instance, neutron scattering studies have shown that water in silica pores can freeze to cubic ice, Ic, instead of hexagonal ice, Ih,[13,17] and a two-dimensional (2-D) ice with rings of eight water molecules forms in a layered nickel chelate complex.[16] Bilayer amorphous ice can form in nanometric pores between parallel, structureless hydrophobic walls modeled by a 9−3 Lennard-Jones potential,[22] and molecular dynamics (MD) simulations suggest that a 2-D rhombohedral ice composed of buckled bilayers of H-bonded H_2O molecules can form in slitlike SiO_2 nanopores modeled with wall−water interactions represented, again, by only a Lennard-Jones potential.[19]

We present here computational MD modeling results for water confined in slitlike nanopores in the layer silicate talc, $Mg_3Si_4O_{10}(OH)_2$, that provide the first evidence for pressure-induced formation of a 2-D ice. The results suggest that elevated pressure may induce formation of previously unknown water structures due to templating by different substrates. The talc 2-D ice has a novel structure resulting from hydrogen bonding between the H_2O molecules and the substrate at elevated pressures. The simulation results also provide detailed structural information about the decompression induced melting mechanism of this 2-D ice structure.

Talc has a so-called TOT layered structure in which layers of linked $[MgO_4(OH)_2]$ octahedra are sandwiched between two layers of SiO_4 tetrahedra linked in six-member rings (Figure 1).[27] The charge-neutral TOT layers are held together by relatively weak van der Waals attractive forces, resulting in the extreme softness of this phase as compared to other silicates. The (001) basal surfaces are quite hydrophobic at ambient conditions because they consist only of oxygens that bridge Si ($Si-O_b-Si$), to which H-bonding is very weak. Importantly, however, the OH groups of the octahedral sheet, which are positioned near the centers of the six-member silicate rings (Figure 1), can be H-bond donors and play a significant role in stabilizing the high pressure 2-D ice.

Talc contains no interlayer water at ambient conditions, but a related hydrated phase, the so-called 10 Å phase, has been experimentally synthesized at high temperatures and pressures[28,29] and may play an important role in controlling the Earth's deep water budget and thermal structure and the chemical and physical behavior in the vicinity of the subduction zones.[30] The 10 Å phase can contain up to two H_2O molecules per formula unit, and our previous MD simulations of a model of this phase based on the ideal talc structure at 5.5 GPa and 750 K yield a novel interlayer structure and provide insight into its stability.[31] The 10 Å phase with its full nominal $2H_2O$ water content is not quenchable to room conditions, but experimental

* Corresponding author. Current address: 166 Everson Hall, University of California at Davis, One Shields Ave., Davis, CA 95616. Phone: (530) 754-8617; fax: (530) 752-0951; e-mail: jwwang@ucdavis.edu.

10.1021/jp045297s CCC: $30.25
Published on Web 07/07/2005

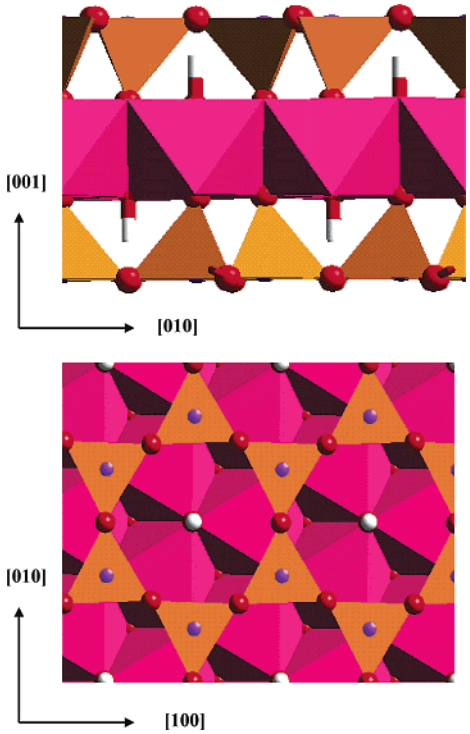

Figure 1. Crystal structure of talc. Top: the side view of a TOT layer. Bottom: the view along [001]. The larger balls (red) are bridging oxygens, O_b; the small balls (purple) are tetrahedral Si; the white balls are hydrogens of OH groups; the triangular shaped polyhedra are Si tetrahedra (dark yellow); and other polyhedra are Mg octahedra (pink).

results show that a phase with less water (0.67−1.0 per formula unit) remains stable after quenching.

Ab initio total energy calculations of hydrated talc with one interlayer water molecule per formula unit show that water molecules are only loosely bound midway between the talc layers with their oxygen atoms positioned above the centers of the six-member silicate rings.[25] Our MD simulations of the compositions with 0.67 and 1.0 H_2O molecules per formula unit are consistent with these results and demonstrate that such systems are not only stable at high temperatures and pressures but remain stable under ambient conditions and yield powder X-ray diffraction patterns in good agreement with experimental observations.[31,32] Although the most recent experimental NMR and XRD work on the 10 Å phase[33,34] suggest that its structure may not consist of just talc + water, the focus here is on the behavior of the interlayer water substructure, which all experimental studies show to be present. The MD simulations described here are for the $Mg_3Si_4O_{10}(OH)_2 + 2H_2O$ composition, which has one water molecule for each six-membered siloxane ring.

Materials and Methods

The initial substrate structure for the MD simulations was that of talc (triclinic, $C\bar{1}$; Figure 1),[27] and all simulations used the recently developed *CLAYFF* force field[35] to describe all interatomic interactions. NPT−ensemble MD simulation of bulk talc at ambient conditions reproduces the $C\bar{1}$ structure well, yielding the crystallographic cell dimensions within 0.8% of the experimental values.[31] The TOT layer structure is also reproduced well, with a computed displacement of about 1.8 Å along the layer plane between the two tetrahedral sheets of a single TOT layer. The stacking of the TOT layers is also quite well-reproduced, with a computed displacement between adjacent TOT layers of about 1.8 Å along the layer plane, approximately 0.2 Å larger than the value estimated from X-ray data.[27] The computed orientation of the OH groups is perpendicular to the layer plane, as expected for trioctahedral sheet silicates.

For the $Mg_3Si_4O_{10}(OH)_2 + 2H_2O$ composition, the simulation supercells consist of $4a \times 2b \times 2c$ unit cells of talc with a total of 64 water molecules placed initially 0.5 Å above the center of each six-membered siloxane ring. At 750 K and 5.5 GPa, the computed stacking between adjacent TOT layers changes to one in which the Si tetrahedra of one siloxane sheet are located above the center of the six-membered rings across the interlayer, and the water molecules are coordinated by nine O_b atoms. The simulation supercell parameters for the system at these conditions are 21.1480, 18.3046, and 20.2405 Å for *a*, *b*, and *c* and 90, 100, and 90° for α, β, and γ, respectively. The simulations resulting in the 2-D ice structure were all performed at 300 K and used the previous supercell parameters as the starting configuration. To carry out these simulations, the supercell *a*, *b*, α, β, and γ parameters were initially fixed, and the *c* dimension was increased stepwise to adjust the system pressure. All atoms of the simulated systems, including the talc substrate, were considered completely mobile and interacting according to the *CLAYFF* force field.[35] All these interactions were included in the calculation of the total pressure of the simulated systems. However, due to the significant differences in compressibility of the aqueous interlayers (largely hydrostatic) and the substrate talc sheets in the direction normal to the layering and parallel to the layering, the decompression modeling by increasing only the supercell *c* dimension over a wide range causes the computed total system stresses within the plane of the TOT sheets to be less than those normal to the plane. These nonhydrostatic effects can be eliminated by slight modifications of the *a* and *b* cell parameters. Thus, for all lower temperature simulations, an ∼0.05% adjustment of *a* and *b* cell parameters to 21.1403 and 18.3175 Å produced virtually homogeneous stresses and allowed us to use the component of the pressure tensor in the direction normal to the TOT layers (P_{ZZ}) as an indicator of total system pressure acting on interlayer water. In all simulations, the cell angles α, β, and γ were constrained to be 90, 100, and 90°, respectively, the *a* and *b* supercell parameters were held constant, and only the variation of the *c* parameter was used to effectively change the pressure on the interlayer water. This set of modeling parameters was chosen to allow the use of the NVT−ensemble simulations that simplify the final analysis of the MD-generated atomic trajectories and visualization of the resulting interlayer structures. The constant-volume approach with a fixed cell shape does not introduce significant limitations on the resulting layer stacking and interlayer structures because all atoms are completely free to move during the simulations.

The simulations used 3-D periodic boundary conditions, the Nosé−Hoover thermostat, standard MD algorithms,[36] and simulation protocols previously described.[31,37−43] All energy expressions and interatomic interaction parameters were taken from *CLAYFF*,[35] except for the charge on apical oxygen atoms (Si−O−Mg; $q_{Oa} = -1.2825$), which was not defined in the original *CLAYFF* set of force field parameters. For water molecules, the flexible version of the simple point charge (SPC) potential was used.[44,45] This potential has been thoroughly tested in numerous molecular simulations of aqueous systems at high temperatures and pressures.[46−48]

Structural relaxation of each model with the predetermined supercell parameters was achieved via the following sequence. Initially, the positions of all Mg atoms were fixed, and all other

atoms of the TOT layers and the interlayer H_2O molecules were allowed to fully relax under energy minimization. This was followed by a relatively short (50 ps) NVT−ensemble MD run to allow the water molecules to relax at 300 K. Then, the Mg atoms were released, and the energy minimization and NVT−ensemble MD runs were repeated with all atoms of the system free to relax. These optimized structures were then used as the starting configurations for the final NVT−ensemble MD simulations. Each system was allowed to equilibrate for 100 ps of MD simulation, and the final equilibrium dynamic trajectory was recorded for 350 ps at 10 fs intervals. A time step of 1.0 fs was used for all MD runs except for the initial 750 K and 5.5 GPa simulation (0.5 fs).

For structural analysis, density profiles for the oxygen (O_{H2O}) and hydrogen (H_{H2O}) atoms of H_2O molecules in the direction perpendicular to the TOT layer were calculated for each simulation by averaging over the entire 350 ps equilibrium MD trajectory. The planes defined by the average positions of the basal oxygen atoms of one of the tetrahedral sheets (O_b) were taken as the origin ($z = 0$). Atomic density contour maps for O_{H2O}, H_{H2O}, and O_b were calculated to visualize the final computed interlayer ordering, site occupancy, and H-bonding of the interlayer H_2O molecules. These maps were obtained as time averages by summing over all instantaneous positions of the specific atom types across the entire MD trajectory and are projected onto planes parallel to the TOT layers.[37,40] The self-diffusion coefficients of the interlayer water molecules were calculated from the mean square displacement of O_{H2O} according a standard statistical−mechanical formalism.[49] The statistical error in the computed diffusion coefficients is estimated to be about 10−15%. The instantaneous pressure tensor of the simulated systems was calculated from the virial theorem[34]

$$\boldsymbol{P} = \frac{1}{V}[\sum_i m_i \mathbf{v}_i \mathbf{v}_i^T + \sum_i \mathbf{r}_i \mathbf{f}_i^T] \quad (1)$$

where V is the volume of the simulation supercell, m_i is the mass of the atom i, and $\mathbf{v}_i$, $\mathbf{r}_i$, and $\mathbf{f}_i$ are, respectively, its instantaneous velocity, its position, and the force acting on it from all other atoms in the system. The instantaneous hydrostatic pressure was then calculated from the trace of the pressure tensor as

$$P = 1/3(P_{XX} + P_{YY} + P_{ZZ}) \quad (2)$$

The statistical errors of the pressure calculation were estimated by the method of block averaging.[36] In this procedure, each equilibrium trajectory was divided into 14, 25 ps long blocks, and the average pressure of each block was calculated. The errors in pressure were then estimated as one standard deviation of the block averages. These errors range from 0.07 GPa at the highest pressure to 0.03 GPa at the lowest pressure and are quite acceptable for the analysis of the computed results and their interpretation in terms of the predicted phase transition.

Results and Discussion

Confined Water Structure. At 5.5 GPa and 750 K, the water molecules of the model of the 10 Å phase are located 1.2 Å above the centers of all six-membered rings and coordinated by nine O_b atoms (six from one TOT sheet and three from the other sheet) and one OH group of the Mg-octahedra (Figures 2a and 3a).[31] The average O−H···O_{H2O} H-bond angle is ∼180°, and its length is 2.1 Å, well within the range for H-bonds.

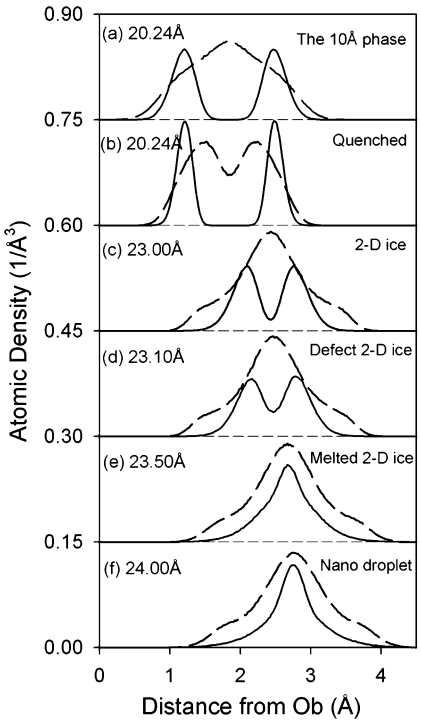

Figure 2. Atomic density profiles for water in talc interlayers at different c-dimensions. Solid lines are O_{H2O}, and dashed lines are H_{H2O}. (a) 20.24 Å, 750 K, 5.49 (±0.07) GPa; (b) 20.24 Å, 3.45 (±0.04) GPa; (c) 23.00 Å, 0.45 (±0.04) GPa; (d) 23.10 Å, 0.45 (±0.06) GPa; (e) 23.50 Å, 0.45 (±0.06) GPa; and (f) 24.00 Å, 0.36 (±0.03) GPa. The systems (b−f) are all at 300 K.

H-bond donation from the OH groups to O_{H2O} plays a major role in stabilizing the structure. The water molecules in the interlayer are separated from each other and do not interact significantly. The average dipole vector of the H_2O molecules is oriented about 30° to the layer plane, but the mean H-position is at the center of the interlayer (Figure 2a). Although some short-lived and strongly distorted H-bonds may form between H_{H2O} and the basal oxygen atoms of the siloxane sheets, there are no clearly preferred H_{H2O} positions in the interlayer structure (Figure 3a). This results in almost ideally circular atomic density contours of H_{H2O} around O_{H2O}, indicating almost free molecular libration and high H_2O orientational disorder at high temperature.

Quenching from 750 to 300 K at constant volume ($c = 20.24$ Å) decreases the interlayer pressure from 5.5 to 3.45 GPa, but the layer stacking does not change, and the water molecules remain in the same positions with the same 9-O_b and 1-HO coordination. However, the distributions of the H_{H2O} and O_{H2O} positions perpendicular the layer are much narrower (Figure 2b) at ambient temperature. The average H_2O dipole vector is oriented at about 20° to the layer plane, and the H_{H2O} atoms show increased site occupancy ordering, as expected at lower temperatures (Figure 3b). There are six preferred H_{H2O} sites positioned exactly on the projections of the O_{H2O}−O_b vectors (Figure 3b), and this configuration indicates increased stability of H-bonds donated by the interlayer water molecules to the siloxane O_b. On the 350 ps time scale of our simulations, individual water molecules do not occupy the six possible orientations with equal probability at every individual site. This occurs because the water molecules are not completely isolated from each other, and the interference among their H-bonds with the O_b atoms causes local orientational heterogeneity on a time scale of approximately 0.5 ns. However, if the H_{H2O} positions are averaged over all individual sites, the positions along all

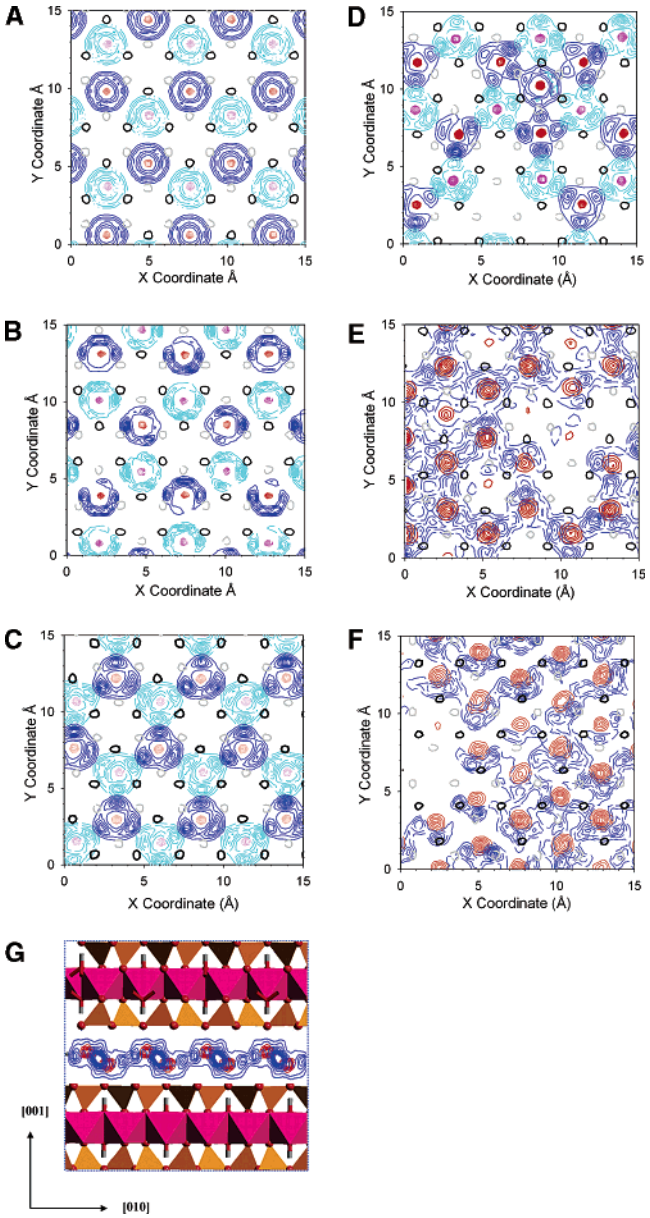

Figure 3. Atomic density contour maps at different pressures for water between the talc layers. The solid darker and lighter open circles (black and gray) are the bridging oxygen atoms (O_b) in the upper and lower neighboring TOT layers across the interlayer. Darker (or red) contours are oxygen atoms of water molecules. In the cases where two sublayers of water are present, the thin solid contours (or blue) are hydrogen atoms of the water molecules close to the upper TOT layer, and the dashed (or cyan) contours are for those close to the lower TOT layer. In cases with a single layer of water, the thin contours (or red) are oxygen atoms of water, and the dashed contours (or blue) are hydrogen atoms of water. The conditions for systems (a−f) are the same as (a−f) in Figure 2. (g) Side view of the two sublayers of the 2-D ice structure, corresponding to the well-ordered conditions of Figures 2(c) and 3(c).

six directions are equally occupied. H-bonding from the OH groups to O_{H2O} continues to play a significant role in stabilizing the structure. With a further pressure decrease (increasing the *c*-axis dimension), the distance from the water molecules to the basal O_b atoms increases, the density profiles of the two sublayers of water approach each other and eventually merge, and the interaction among water molecules begins to play a more prominent role (Figure 2). The layer stacking between adjacent TOT layers is the same as at 750 K and 5.5 GPa and retains this configuration in all simulations.

At $c = 23.00$ Å ($P = 0.45$ GPa), the interlayer water assumes a buckled two-dimensional (2-D) ice-like structure with a complete and highly ordered H-bonding configuration among interlayer water molecules (Figures 2c and 3c,g). In this configuration, each water molecule is coordinated by six O_b atoms of one basal siloxane sheet and three water molecules. The water molecules are arranged in a buckled hexagonal array in the $a-b$ plane with two sublayers (Figures 2c and 3c,g). Each H_2O molecule has four H-bonds, accepting one from an OH group and one from another water molecule and donating one to an O_b and one to another water molecule. There are nine possible sites to be occupied by the two H-atoms of each water molecule. Three of these donate H-bonds to other water molecules and are 1/3 occupied. Six others donate H-bonds to O_b and are 1/6 occupied (Figure 3c). The H-positions of both types of H-sites strongly overlap in the $a-b$ projection, and the resulting atomic density map contains three broad asymmetric H_{H2O} maxima around each O_{H2O} (Figure 3c).

The resulting interlayer H-bond network obeys the so-called ice rules,[9,50,51] according to which each water molecule has four H-bonds, accepting two and donating two. This coordination environment and H-bond network is similar in some respects to that of ice Ih,[52−54] but for the talc 2-D ice, both external pressure and H-bond interaction with O_b and OH groups are essential for structural stabilization. The OH groups provide a hexagonal array of H-bond donors, comparable to that in ice Ih.[52−54] For each H_2O, the H-bonded neighbors form a distorted tetrahedron, as in ice Ih.

In ice Ih, the H-atoms of each H_2O are disordered over four positions that are located between the central molecule and its four neighbors. In contrast, in the talc 2-D ice, the H-atoms are disordered over nine positions that are located between the molecule and six O_b and three neighboring H_2O. The longest distance in the $a-b$ plane between adjacent H_2O molecules is about 6.05 Å, somewhat larger than the value of 5.30 Å in the (001) layers of ice Ih.[9] The buckled layer of the 2-D ice has rhombic symmetry as in a single (001) layer of ice Ih. In ice Ih, each buckled layer can accept or donate H-bonds from or to the neighboring buckled layers, whereas in the 2-D ice, the buckled layer accepts external H-bonds only from the OH groups.

This 2-D ice structure is quite different from those previously reported in terms of the local structural environments, H-bonding configuration, and substrate−water interaction. For the 2-D ice in the layered nickel(II) chelate complexes, the substrate molecules provide geometric constraints on the water layer substructure and on the sites on the organic molecules to which the water molecules are H-bonded.[16] In contrast, for water molecules confined in a hydrophobic slitlike pore represented by only a 6−12 Lennard-Jones wall−water potential at room temperature, there are no strong interaction sites on the substrate to direct the orientation of water molecules, and no H-bonds can form with the substrate surfaces.[19] Rather, the water molecules interact only among themselves. MD simulations suggest that a 2-D rhombohedral ice composed of buckled bilayers of H-bonded H_2O molecules can form in such slitlike nanopores that mimic SiO_2 walls but interact with water molecules via only a Lennard-Jones potential.[19] Bilayer amorphous ice can also form between parallel structureless hydrophobic walls modeled by a 9−3 Lennard-Jones potential.[22]

Interlayer Melting in Hydrous Talc. As the *c*-axis dimension increases from 23.00 to 23.50 Å at 300 K for the talc−$2H_2O$ system, the computed pressure remains constant at ∼0.45 GPa (Figure 4), and the 2-D interlayer ice-like structure becomes

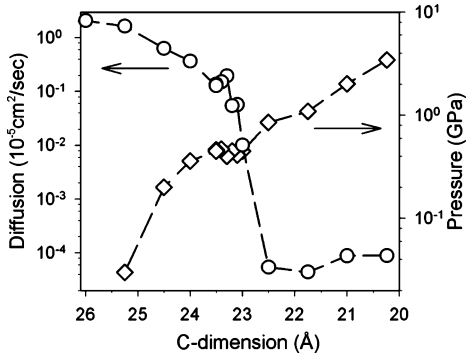

Figure 4. Computed pressure and self-diffusion coefficients of interlayer water. The circles and squares are calculated data points, and the connecting lines are plotted as eye guides.

progressively more disordered and finally melts (Figures 2−4). A first-order phase transition can be identified by a discontinuity of the first derivatives of free energy with respect to temperature and pressure at the transition point. As shown in Figure 4, the *c*-dimension (volume) can change from 23.00 to 23.50 Å, while the system maintains a constant pressure of 0.45 GPa, which means that the volume is discontinuous with respect to system pressure

$$V = \left(\frac{\partial G}{\partial P}\right)_T \tag{3}$$

This remarkable constancy of computed pressures over a significant range of volumes suggests that a first-order phase transition is indeed observed in our simulations.

Upon further expansion, melting is initiated by migration of a few water molecules to interstitial positions within six-membered rings of the ice structure and concomitant formation of vacant sites in the 2-D ice lattice (Figures 2d and 3d). This structure can be considered a defective 2-D ice. The interstitial H_2O is located at the center of the interlayer region along the *c*-direction and is coordinated by three O_b from one TOT sheet at about 2.9 Å, three O_b from the other TOT sheet at about 2.9 Å, and six water molecules at 3.1 Å. Three of these H_2O molecules are from one sublayer, and three are from the other (Figure 3d). The H-bonding opportunities for the interstitial molecule with the six nearest neighbor waters are equal, resulting in six preferred positions for the hydrogen atoms. It forms no H-bonds with the O_b substrate atoms. The six neighboring water molecules to the interstitial H_2O are coordinated by four other water molecules and H-bonded to them. The presence of the interstitial H_2O causes outward displacement of the H-maxima within the six-membered ring (distortion of the H-bonds) due to H−H repulsion (Figure 3d). The three water molecules surrounding the vacancy are H-bonded to two other water molecules and two O_b substrate atoms, resulting in four H_{H2O} density maxima (Figure 3d).

The next definable stage of disordering with increasing decompression (increasing *c*-dimension) involves the formation of progressively larger numbers of vacancies and interstitial molecules and the transformation of the bilayer structure into a single layer with the O_{H2O} and H_{H2O} density maxima at the center of the interlayer (Figures 2e and 3e). Over the course of the 350 ps MD simulations for the model systems with $23.00 \leq c \leq 23.5$ Å, some of the water molecules become delocalized, and overall, their coordination and H-bonding become distorted, statically and dynamically disordered, and much more liquidlike than observed in the 2-D ice (Figure 3e). Some H_2O molecules remain near their initial ice sites and interstitial positions, and the interaction between the water and the substrate talc atoms remains significant. There are two principal types of water sites, one above or below the center of a six-membered siloxane ring and one above or below silicate tetrahedra.

At $c = 24.0$ Å, the interlayer is fully melted (Figure 2f and 3f), and the system pressure decreases to 0.36 GPa (Figure 4). Under this condition, a significant fraction of the interlayer space is unoccupied by water, and the H_2O molecules are densely packed and H-bonded to each other. The 0.36 GPa is still much higher than the pressure of equilibrium (3.5 KPa) between bulk water and its vapor at the same temperature of 300 K.[9] To achieve room pressure at 300 K, more than half of the interlayer space would have to be unoccupied. This positive pressure is caused by the hydrophobic interaction between water and talc in combination with the strong interaction among water molecules. Complete melting is indicated by the transition from a bilayer to a single layer water structure (Figure 2). In the course of the MD simulations, melting can be observed as an equilibrium involving simultaneous presence of the 2-D ice phase in one interlayer and liquid water in the adjacent interlayer of the same simulation supercell. Figure 2 shows density profiles of water in one of these two interlayers. Despite being under the same pressure, the water molecules of one layer are liquidlike (similar to Figure 2e), whereas those of the other could retain the 2-D ice structure with two sublayers (similar to Figure 2c). Only after both interlayers melt does the system pressure decrease again with decreasing density.

The melting phase transition also causes large increases in the water self-diffusion coefficients (Figure 4) in the interlayer. For the quenched 10 Å phase at 300 K and conditions resulting in ordered 2-D ice with pressures from 0.45 to 3.4 GPa, the diffusion coefficients are of the order of 10^{-9} cm^2/s and change little with pressure. Upon melting, the diffusion coefficients jump by 3 orders of magnitude over a *c*-axis range between 23.00 and 23.50 Å and continue to increase further with increasing volume.

The computed decompressional melting of the 2-D ice between talc layers is quite different from the melting of bulk ice Ih. The 2-D ice melting follows the three steps described previously, whereas the onset of melting of ice Ih does not create defects.[55,56] Rather, it involves simultaneous translational and orientational disordering of the molecules,[55,56] and these changes can be understood in terms of disruption of the 3-D H-bonding network.[57] Previous MD computer simulations have shown that bulk ice melts from crystallite surfaces toward the interior.[55,56]

Acknowledgment. This research was supported by DOE Basic Energy Sciences Grant DEFGO2-00ER-15028. Computation was partially supported by the National Computational Science Alliance (Grant EAR 990003N) and NCSA SGI/CRAY Origin2000 computers and Cerius2-4.0 software package from Accelrys were used. J.W. also acknowledges the fellowship from the University of Illinois at Urbana-Champaign. Fruitful discussions with M. D. Welch (The Natural History Museum, London) and Prof. Brian Phillips (SUNY Stony Brook) about the 10 Å phase and R. T. Cygan (Sandia National Lab) about force-field parametrization are most gratefully acknowledged.

References and Notes

(1) Raviv, U.; Laurat, P.; Klein, J. *Nature* **2001**, *413*, 51.

(2) Zhu, Y.; Granick, S. *Phys. Rev. Lett.* **2001**, *87*, 096104.

(3) Mitra, S.; Mukhopadhyay, R.; Tsukushi, I.; Ikeda, S. *J. Phys.: Condens. Matter* **2001**, *13*, 8455.

(4) Spohr, E.; Hartnig, C.; Gallo, P.; Rovere, M. *J. Mol. Liq.* **1999**, *80*, 165.

(5) Hartnig, C.; Witschel, W.; Spohr, E. *J. Phys. Chem. B* **1998**, *102*, 1241.
(6) Antognozzi, M.; Humphris, A. D. L.; Miles, M. *J. Appl. Phys. Lett.* **2001**, *78*, 300.
(7) Bergman, R.; Swenson, J. *Nature* **2000**, *403*, 283.
(8) Senapati, S.; Chandra, A. *J. Phys. Chem. B* **2001**, *105*, 5106.
(9) Eisenberg, D.; Kauzmann, W. *The structure and properties of water*; Oxford University Press: New York, 1969.
(10) Dmitriev, V. P.; Rochal, S. B.; Toledano, P. *Phys. Rev. Lett.* **1993**, *71*, 553.
(11) Mishima, O.; Stanley, H. E. *Nature* **1998**, *396*, 329.
(12) Bellissent-Funel, M.-C. *J. Phys.: Condens. Matter* **2001**, *13*, 9165.
(13) Dore, J. *Chem. Phys.* **2000**, *258*, 327.
(14) Nandi, N.; Bhattacharyya, K.; Bagchi, B. *Chem. Rev.* **2000**, *100*, 2013.
(15) Robinson, G. W.; Zhu, S.-B.; Singh, S.; Evans, M. W. *Water in Biology, Chemistry, and Physics. Experimental Overviews and Computational Methodologies*; World Scientific Publishing Co. Pte. Ltd.: Singapore, 1996.
(16) Janiak, C.; Scharmann, T. G. *J. Am. Chem. Soc.* **2002**, *124*, 14010.
(17) Bellissent-Funel, M.-C. *J. Mol. Liq.* **2002**, *96*−*97*, 287.
(18) Slovák, J.; Tanaka, H.; Koga, K.; Zeng, X. C. *Phys. A* **2003**, *319*, 163.
(19) Zangi, R.; Mark, A. E. *J. Chem. Phys.* **2003**, *119*, 1694.
(20) Zangi, R.; Mark, A. E. *Phys. Rev. Lett.* **2003**, *91*, 025502.
(21) Bai, J.; Su, C.-R.; Parra, R. D.; Zeng, X. C.; Tanaka, H.; Koga, K.; Li, J.-M. *J. Chem. Phys.* **2003**, *118*, 3913.
(22) Koga, K.; Tanaka, H.; Zeng, X. C. *Nature* **2000**, *408*, 564.
(23) Slovák, J.; Koga, K.; Tanaka, H. *Phys. Rev. E* **1999**, *60*, 5833.
(24) Meyer, M.; Stanley, H. E. *J. Phys. Chem. B* **1999**, *103*, 9728.
(25) Bridgeman, C. H.; Buckingham, A. D.; Skipper, N. T.; Payne, M. C. *Mol. Phys.* **1996**, *89*, 879.
(26) Bridgeman, C. H.; Skipper, N. T. *J. Phys.: Condens. Matter* **1997**, *9*, 4081.
(27) Rayner, J. H.; Brown, G. *Clays Clay Miner.* **1973**, *21*, 103.
(28) Yamamoto, K.; Akimoto, S. *Am. J. Sci.* **1977**, *277*, 288.
(29) Chinnery, N. J.; Pawley, A. R.; Clark, S. M. *Science* **1999**, *286*, 940.
(30) Manning, C. E. *Earth Planet. Sci. Lett.* **2004**, *223*, 1.
(31) Wang, J.; Kalinichev, A. G.; Kirkpatrick, R. J. *Earth Planet. Sci. Lett.* **2004**, *222*, 517.
(32) Fumagalli, P.; Stixrude, L.; Poli, S.; Snyder, D. *Earth Planet. Sci. Lett.* **2001**, *186*, 125.
(33) Pawley, A. R.; Welch, M. D. *EOS Trans. Am. Geophys. Union* **2004**, *85*, Fall Meeting Suppl., Abstract T43E-06.
(34) Phillips, B. L. 2005, personal communication.
(35) Cygan, R. T.; Liang, J.-J.; Kalinichev, A. G. *J. Phys. Chem. B* **2004**, *108*, 1255.
(36) Allen, M. P.; Tildesley, D. J. *Computer Simulation of Liquids*, Clarendon Press: Oxford, 1987.
(37) Wang, J.; Kalinichev, A. G.; Kirkpatrick, R. J. *Geochim. Cosmochim. Acta* **2004**, *68*, 3351.
(38) Wang, J.; Kalinichev, A. G.; Amonette, J. E.; Kirkpatrick, R. J. *Am. Mineral.* **2003**, *88*, 398.
(39) Kirkpatrick, R. J.; Kalinichev, A. G.; Wang, J.; Hou, X.; Amonette, J. E. In *The Application of Vibrational Spectroscopy to Clay Minerals and Layered Double Hydroxides, CMS Workshop Lectures*; Kloprogge, J. T., Ed.; The Clay Minerals Society: Aurora, CO, 2004; Vol. 13, p 239.
(40) Kalinichev, A. G.; Kirkpatrick, R. J. *Chem. Mater.* **2002**, *14*, 3539.
(41) Wang, J. W.; Kalinichev, A. G.; Kirkpatrick, R. J.; Hou, X. Q. *Chem. Mater.* **2001**, *13*, 145.
(42) Cygan, R. T. *Rev. Mineral. Geochem.* **2001**, *42*, 1.
(43) Kalinichev, A. G.; Kirkpatrick, R. J.; Cygan, R. T. *Am. Mineral.* **2000**, *85*, 1046.
(44) Berendsen, H. J. C.; Postma, J. P. M.; van Gunsteren, W. F.; Hermans, J. In *Intermolecular Forces*; Pullman, B., Ed.; Riedel: Dordrecht, The Netherlands, 1981; p 331.
(45) Teleman, O.; Jönsson, B.; Engström, S. *Mol. Phys.* **1987**, *60*, 193.
(46) Brodholt, J. P.; Wood, B. J. *J. Geophys. Res.* **1993**, *98B*, 519.
(47) Chialvo, A. A.; Cummings, P. T. *Adv. Chem. Phys.* **1999**, *109*, 115.
(48) Kalinichev, A. G. *Rev. Mineral. Geochem.* **2001**, *42*, 83.
(49) McQuarrie, D. A. *Statistical Mechanics*; Harper and Row Publishers: New York, 1976.
(50) Pauling, L. *J. Am. Chem. Soc.* **1935**, 57.
(51) Bernal, J. D.; Fowler, R. H. *J. Chem. Phys.* **1933**, *1*, 515.
(52) Peterson, S. W.; Levy, H. A. *Acta Crystallogr.* **1957**, *10*, 70.
(53) Lonsdale, D. K. *Proc. Royal Soc. London, Ser. A* **1958**, *247*, 424.
(54) Goto, A.; Hondoh, T.; Mae, S. *J. Chem. Phys.* **1990**, *93*, 1412.
(55) Weber, T. A.; Stillinger, F. H. *J. Chem. Phys.* **1984**, *80*, 438.
(56) Weber, T. A.; Stillinger, F. H. *J. Phys. Chem.* **1983**, *87*, 4277.
(57) Kroes, G.-J. *Surf. Sci.* **1992**, *275*, 365.